

Generating Potent C–H PCET Donors: Ligand-Induced Fe-to-Ring Proton Migration from a Cp*Fe^{III}–H Complex Demonstrates a Promising Strategy

Dirk J. Schild,[†] Marcus W. Drover,[†] Paul H. Oyala, and Jonas C. Peters*



Cite This: <https://dx.doi.org/10.1021/jacs.0c09363>



Read Online

ACCESS |



Metrics & More

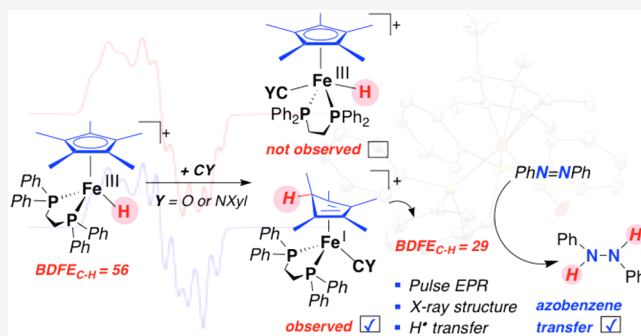


Article Recommendations



Supporting Information

ABSTRACT: Highly reactive organometallic species that mediate reductive proton-coupled electron transfer (PCET) reactions are an exciting area for development in catalysis, where a key objective focuses on tuning the reactivity of such species. This work pursues ligand-induced activation of a stable organometallic complex toward PCET reactivity. This is studied via the conversion of a prototypical Cp*Fe^{III}–H species, [Fe^{III}(η^5 -Cp*)(dppe)H]⁺ (Cp* = C₅Me₅[−], dppe = 1,2-bis(diphenylphosphino)ethane), to a highly reactive, S = 1/2 ring-protonated *endo*-Cp*H–Fe relative, triggered by the addition of CO. Our assignment of the latter ring-protonated species contrasts with its previous reported formulation, which instead assigned it as a hypervalent 19-electron hydride, [Fe^{III}(η^5 -Cp*)(dppe)(CO)H]⁺. Herein, pulse EPR spectroscopy (^{1,2}H HYSCORE, ENDOR) and X-ray crystallography, with corresponding DFT studies, cement its assignment as the ring-protonated isomer, [Fe^I(*endo*- η^4 -Cp*H)(dppe)(CO)]⁺. A less sterically shielded and hence more reactive *exo*-isomer can be generated through oxidation of a stable Fe⁰(*exo*- η^4 -Cp*H)(dppe)(CO) precursor. Both *endo*- and *exo*-ring-protonated isomers are calculated to have an exceptionally low bond dissociation free energy (BDFE_{C–H} ≈ 29 kcal mol^{−1} and 25 kcal mol^{−1}, respectively) cf. BDFE_{Fe–H} of 56 kcal mol^{−1} for [Fe^{III}(η^5 -Cp*)(dppe)H]⁺. These weak C–H bonds are shown to undergo proton-coupled electron transfer (PCET) to azobenzene to generate diphenylhydrazine and the corresponding closed-shell [Fe^{II}(η^5 -Cp*)(dppe)CO]⁺ byproduct.



INTRODUCTION

Proton-coupled electron transfer (PCET) reactions have emerged as powerful strategies for mediating sundry reductive transformations in organic synthesis, with clever new approaches being discovered to generate in situ highly reactive H atom surrogates as intermediates.^{1–3} Reactive fragments with weak element-hydrogen (E–H) bonds have thus been targeted to facilitate hydrogen atom delivery, revealing desirable substrate reductions that are fascinating in scope.^{1,2,4} As a salient example, dissolution of SmI₂ in H₂O/THF mixtures confers coordination-induced bond-weakening in the resulting [Sm(H₂O)_n]²⁺ complex to provide weak and hence highly reactive O–H bonds (BDFE_{O–H} ≈ 26 kcal mol^{−1});^{1h} such species can be employed toward substrate reductions such as ketones to alcohols and anthracene to dihydroanthracene⁵ and also toward catalytic N₂ fixation to NH₃ in the presence of a Mo catalyst.⁶

As an outgrowth of our own mechanistic studies of Fe-mediated N₂ fixation, we recently reported the rigorous characterization of a highly reactive [Cp*(*endo/exo*- η^4 -Cp*H)-Co]⁺ (Cp* = C₅Me₅[−]) species (BDFE_{C–H} < 29 kcal mol^{−1} for the *exo*-analogue), generated in situ via ring protonation of decamethylcobaltocene, Cp*₂Co.^{7,8} Relatedly, we have exam-

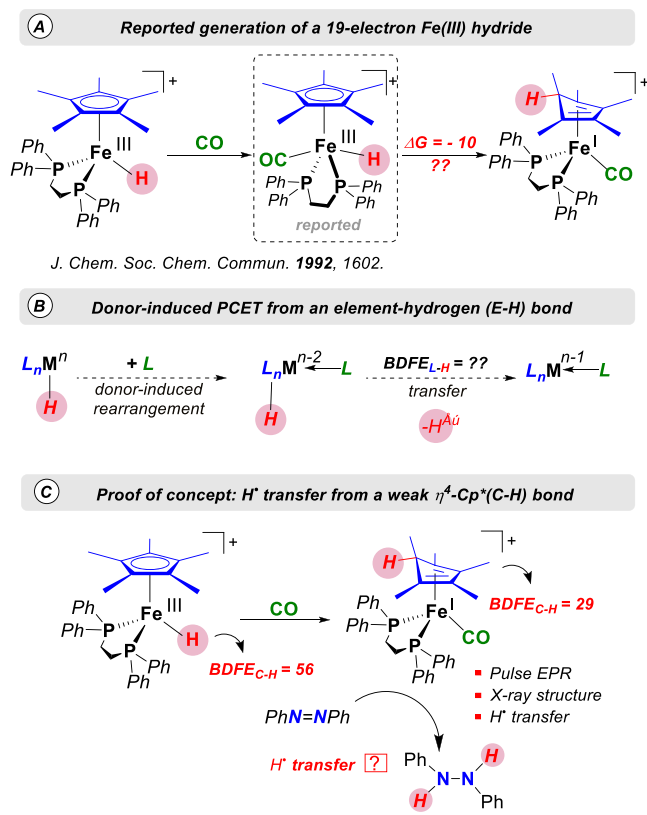
ined an Fe(III) indenide hydride [Fe^{III}(η^5 -Ind)(depe)H]⁺ (Ind = C₈H₇[−], depe = 1,2-bis(diethylphosphino)ethane) and its low temperature isomerism to give a η^6 -indene complex, [Fe(η^6 -IndH)(depe)]⁺, (BDFE_{X–H} = 50 kcal mol^{−1}; X = Fe or C).⁹

The highly reactive nature of these ring-protonated species has frustrated independent studies of their reactivity profiles toward exogenous substrates. We hence targeted a related system wherein a reactive ring–C–H PCET donor might be generated in solution, via association of a ligand to the metal to cause concomitant isomerization of a metal-bound hydride to a Cp*-ring position. Such a strategy would, in principle, enable two unreactive partners to reside in solution, with a net PCET reaction being triggered by addition of a donor ligand L (see Chart 1).

With this goal in mind, we turned to a known iron(III) hydride half-sandwich complex, [Fe^{III}(η^5 -Cp*)(dppe)H]⁺[1]⁺,

Received: August 31, 2020

Chart 1. (A) Reported Generation of a 19-Electron Fe^{III}-H,¹¹ Reassigned Herein; (B) Generalized Donor-Induced PCET; (C) Donor-Induced PCET Described in This Study^a



^aBDFE values (calculated by DFT) are in kcal mol⁻¹.

(Cp* = C₅Me₅⁻, dppe = 1,2-bis(diphenylphosphino)ethane), first prepared by Lapinte and co-workers in 1992.¹⁰ Complex [1]⁺ was reported to undergo associative binding of CO to provide the 19-electron hydride [Fe^{III}(η⁵-Cp*)(dppe)(CO)-H]⁺ ([2]⁺), the latter having been characterized by X-band EPR spectroscopy. The reaction was deemed reversible with warming, returning [1]⁺.¹¹

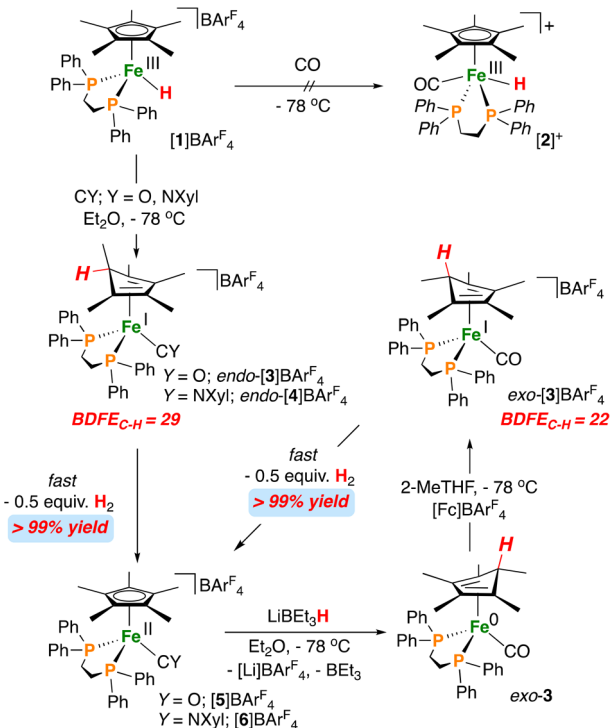
Based on our findings with [Cp*(endo-η⁴-Cp*H)Co]⁺ and [Fe(η⁶-IndH)(depe)]⁺, we wondered whether [2]⁺ would be best described as [Fe^I(η⁴-Cp*H)(dppe)(CO)]⁺, which would occur via proton migration to the ring upon CO binding. Herein, we use a range of methods, including crystallography and various EPR techniques, with corresponding DFT analysis, to establish this is indeed the case. We then demonstrate that an intermolecular PCET reaction is possible, with azobenzene as a model substrate, via this ligand-induced trigger.

RESULTS AND DISCUSSION

We began our study with (re)examining the solution spectroscopy of [Fe^{III}(η⁵-Cp*)(dppe)H]⁺[1]⁺ in the presence of CO. Addition of CO to the ¹H and ²H isotopologues (Fe-H/D) of [1]⁺ results in a change in the EPR spectrum, indicating the formation of a single S = 1/2 species exhibiting rhombic symmetry (g = [2.085, 2.039, 2.004]), parameters that are similar to those previously reported by Lapinte (g = [2.0777, 2.0367, 2.0019], A(³¹P) = ±[48, 50, 50] MHz, and A(¹H) = ±[14, 17, 34] MHz (a_{iso}(¹H) = ±22 MHz)).¹¹ Based on preliminary DFT calculations (vide infra) and the similarity of the proton hyperfine coupling to ring protonated

cobaltocenes,⁴ we posited its structure to be [Fe^I(endo-η⁴-Cp*H/D)(dppe)(CO)]⁺ (endo-isomer confirmed by XRD vide infra), endo-[3-H/D]⁺, rather than the terminal hydride [2]⁺ (Scheme 1).

Scheme 1. Reported Preparation and (Incorrect) Assignment of a 19-Electron Fe(III)-H Complex¹¹ and Synthesis of endo-[3]⁺/[4]⁺ by Addition of CO or CNXyl with Accompanying H₂ Release to Give [5]⁺ and [6]⁺^a



^aBDFE values (calculated by DFT) are in kcal mol⁻¹.

Consumption of [1]⁺ is easily identified by EPR spectroscopy based on the significant shift in the value of g_{max} (Figure 1). Besides coupling to two distinct ³¹P (I = 1/2) nuclei with similar magnitude, significant additional coupling to ¹H is evident when the ¹H and ²H isotopologues are compared, consistent with the presence of a relatively strongly coupled ¹H nucleus (Figure 2). Collection of a series of X-band Davies ENDOR spectra acquired across the EPR envelope of endo-[3-D]⁺ (see the Supporting Information) provides additional data consistent with large couplings to two nonequivalent phosphines (A(³¹P₁) = ±[72, 59, 58] MHz and A(³¹P₂) = ±[49, 42, 51] MHz).

X-band HYSORE spectroscopy of the ¹H and ²H isotopologues was used to determine the hyperfine parameters for the hydride-derived hydrogen nucleus (Figure 2). Simulation of field-dependent HYSORE spectra of endo-[3-H]⁺ reveals a relatively isotropic proton hyperfine tensor, A(¹H) = ±[24, 20, 34.5] MHz (a_{iso}(¹H) = ±26.2 MHz), with a small Euler rotation of the hyperfine tensor relative to the g-tensor of (α, β, γ) = (0, 30, 0)^o. HYSORE spectra of endo-[3-D]⁺ exhibit intense features arising from deuterium which are well simulated by scaling the ¹H hyperfine tensor determined from ¹H HYSORE by the proportion of ¹H/²H gyromagnetic ratios (γ¹H/γ²H = 6.514), with A(²H) = ±[3.7, 3.1, 5.3] MHz. These parameters provide excellent agreement with simu-

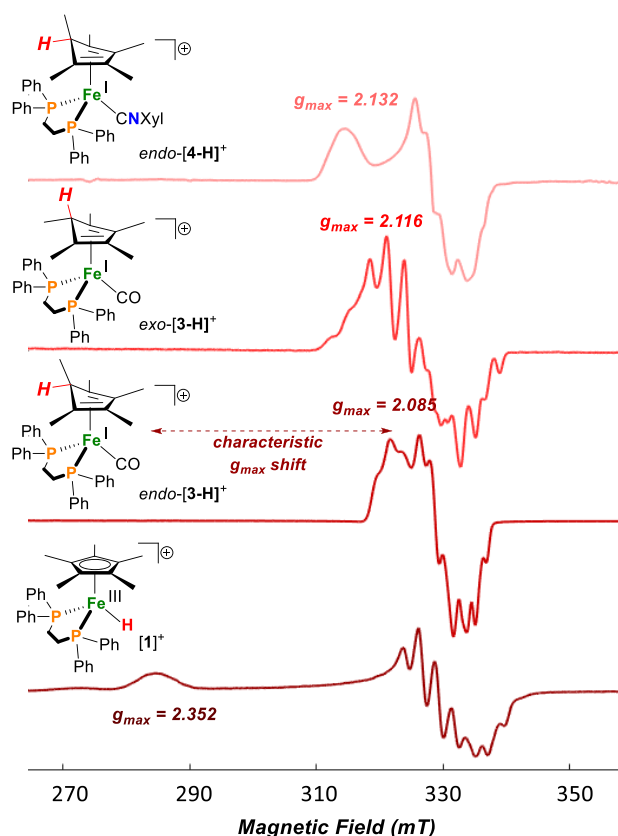


Figure 1. X-band CW-EPR spectra of $[1]^+$, $endo\text{-}[3\text{-H}]^+$, $exo\text{-}[3\text{-H}]^+$, and $endo\text{-}[4\text{-H}]^+$ in 2-MeTHF at 77 K.

lations of the X-band CW-EPR spectra of these two isotopologues.

In contrast to terminal metal-hydrides,¹² the anisotropic component (T) of the ^1H hyperfine of $endo\text{-}[3]^+$, $T(^1\text{H}) = \pm[-2.2, -6.2, 8.3]$ MHz), is considerably smaller, indicating greater distance between the nucleus and Fe-centered spin density. Similarly, low anisotropy is also observed for the $endo\text{-Cp}^*(\text{H})$ protonation product of Cp^*_2Co . The low anisotropy suggests ring-protonation ($endo\text{-}[3]^+$), and not a terminal hydride (i.e., $[2]^+$) species. Hyperfine coupling constants and the predicted anisotropy as calculated by DFT further support the assignment and are independent of the method used (see the Supporting Information).

We also explored the addition of an isocyanide donor, CNXyl (Xyl = 2,6-dimethylphenyl). Treatment of $[1]^+$ with CNXyl at -78°C provides $[\text{Fe}^{\text{I}}(endo\text{-}\eta^4\text{-Cp}^*\text{H})(\text{dppe})(\text{CNXyl})]^+$ ($endo\text{-}[4]^+$) as evidenced by CW X-band EPR spectroscopy at 77 K; $g = [2.132, 2.042, 2.004]$, $A(^{31}\text{P}_1) = \pm[75, 35, 54]$ MHz, and $A(^{31}\text{P}_2) = \pm[76, 64, 64]$ MHz. Simulations of HYSCORE spectra of $endo\text{-}[4\text{-H/D}]^+$ give $A(^1\text{H}) = \pm[17, 22, 32.5]$ MHz, $a_{\text{iso}}(^1\text{H}) = \pm 23.8$ MHz, and $T(^1\text{H}) = \pm[-6.8, -1.8, 8.7]$, which are nearly identical to those discussed above for the $endo\text{-Cp}^*(\text{C-H})$ $\text{Fe}(\text{CO})$ adduct $endo\text{-}[3]^+$. Additional features present in the $(-,+)$ quadrant of HYSCORE of both $endo\text{-}[4\text{-H}]^+$ and $endo\text{-}[4\text{-D}]^+$ can be assigned to hyperfine coupling to ^{14}N in the CNXyl ligand, with $A(^{14}\text{N}) = [7.4, 7.4, 9]$ MHz, a relatively small ^{14}N nuclear quadrupole coupling constant $e^2qQ/h(^{14}\text{N}) = 1.0$ MHz, and a negligible electric field gradient rhombicity $\eta(^{14}\text{N}) \approx 0$, as expected for a triply bonded CN moiety with axial symmetry.¹³

The more stable, neutral $endo/exo$ -species ($endo/exo\text{-}3$) were also prepared. Treatment of $[\text{Fe}^{\text{II}}(\eta^5\text{-Cp}^*)(\text{dppe})(\text{CO})][\text{BAR}^{\text{F}}_4]$ ($[5][\text{BAR}^{\text{F}}_4]$) with LiBEt_3H provides $exo\text{-}[\text{Fe}^0(\eta^4\text{-Cp}^*\text{H})(\text{dppe})(\text{CO})]$ ($exo\text{-}3$) in good yield (Scheme 1). The alternative isomer, $endo\text{-}3$, was prepared via reduction of $endo\text{-}[3]^+$ with Cp_2Co at -78°C .¹¹ The room temperature stability allowed for isolation and growth of crystalline material suitable for single crystal X-ray diffraction. The structures of $exo/endo\text{-}3$ are presented in Figure 3. $Exo\text{-}$ and $endo\text{-}3$ feature an η^4 -diene unit bound to a zerovalent iron center. Notably, the $\text{C}(1)\text{-C}(6)$ bond distance in $endo\text{-}3$ (1.538(3) Å) is slightly longer than that in $exo\text{-}3$ (1.514(2) Å), possibly suggestive of $\text{Fe} \rightarrow \text{C-C}$ (σ^*) donation in the former. Such an interaction is predicted based on the singularly occupied molecular orbitals (SOMOs) of $endo/exo\text{-}[3]^+$ (Figure 4). Two distinct C-H stretches are observed for $exo\text{-}3\text{-H}$ at 2711 and 2612 cm^{-1} that shift to 2009 and 1955 cm^{-1} for $exo\text{-}3\text{-D}$; C-H stretches for $endo\text{-}3\text{-H}$ are not discernible from the bulk C-H stretching region i.e., >2711 cm^{-1} (see the Supporting Information).¹⁴ Similar observations have been made for the pairs: $[\text{Cp}^*(exo\text{-}\eta^4\text{-Cp}^*\text{H})\text{Co}^{\text{II}}]/[\text{Cp}^*(exo\text{-}\eta^4\text{-Cp}^*\text{D})\text{Co}^{\text{II}}]$ ⁸ and $[\text{Cp}(\eta^4\text{-C}_5\text{H}_6)\text{Co}]/[\text{Cp}(exo\text{-}\eta^4\text{-C}_5\text{H}_5\text{D})\text{Co}]$.¹⁵

Despite its exceptionally weak C-H bond, the assignment of $endo\text{-}[3]^+$ could be corroborated by X-ray crystallography (Figure 3) via growth of suitable crystals at low temperature. Gratifyingly, the solid-state structure, which was unobtainable for $[\text{Cp}^*(endo\text{-}\eta^4\text{-Cp}^*\text{H})\text{Co}]^+$, confirms the formation of an $endo\text{-Cp}^*(\text{C-H})$ bond, with metrics associated with a dearomatized five-membered Cp^*H ring that differs from that of a Cp^* anion with elongation along the $\text{C}(1)\text{-C}(5)$ and $\text{C}(1)\text{-C}(2)$ vectors [$1.51(1)/1.53(1)$ Å] from ca. 1.42 Å (average C-C bond distances in $[7]^+$, vide infra), signifying new C-C single bonds. The low temperature stability of $endo\text{-}[3]^+$ likely derives from a high degree of steric shrouding of the reactive ring-bound H atom via phenyl rings from the dppe ligand.

Next, we sought to generate the alternative, and presumably more reactive, exo -isomer wherein steric shrouding by dppe is far less prominent. Oxidation of neutral $exo\text{-}3$ with $[\text{Fc}]\text{BAR}^{\text{F}}_4$ at -78°C provides green solutions of reactive $exo\text{-}[3]^+$ that can be analyzed by EPR spectroscopy. From the CW data, we assign two conformational isomers of $exo\text{-}[3]^+$ (A and B), both with rhombic symmetry (Figure 5): A with $g = [2.116, 2.073, 1.997]$ and another, B with $g = [2.093, 2.045, 2.013]$ that presumably differ by rotation of the Cp^*H ligand. The potential presence of multiple conformers is supported by DFT, as four distinct minima are found within 2 kcal mol^{-1} upon Cp^*H rotation. The exact nature of the conformers present in solution could not be determined, due to the small differences in energies and predicted ^1H hyperfine tensors (see the Supporting Information). Least-squares optimization of simulations of the X-band CW spectra converged at relative populations of 0.6:0.4 for conformers A:B, indicating that the two conformations are indeed of similar relative energies. Simulations of $^2\text{H}\text{-}^1\text{H}$ difference ENDOR spectra of this mixture of $exo\text{-}[3]^+$ products provided constraints on the ^2H (and by proxy ^1H) hyperfine couplings, with higher frequency ENDOR providing the same for ^{31}P hyperfine couplings for the two conformers in the above CW simulations, with $A(^1\text{H}) = \pm[85, 84, 83]$ MHz, $a_{\text{iso}}(^1\text{H}) = \pm 84$ MHz, $T(^1\text{H}) = \pm[1, 0, -1]$, $A(^{31}\text{P}_1) = \pm[96, 88, 47]$ MHz, and $A(^{31}\text{P}_2) = \pm[78, 75, 63]$ MHz for conformer A and $A(^1\text{H}) = \pm[76, 74, 70]$ MHz, $a_{\text{iso}}(^1\text{H}) = \pm 73$ MHz, $T(^1\text{H}) = \pm[3, 1, -3]$, $A(^{31}\text{P}_1) = \pm[46,$

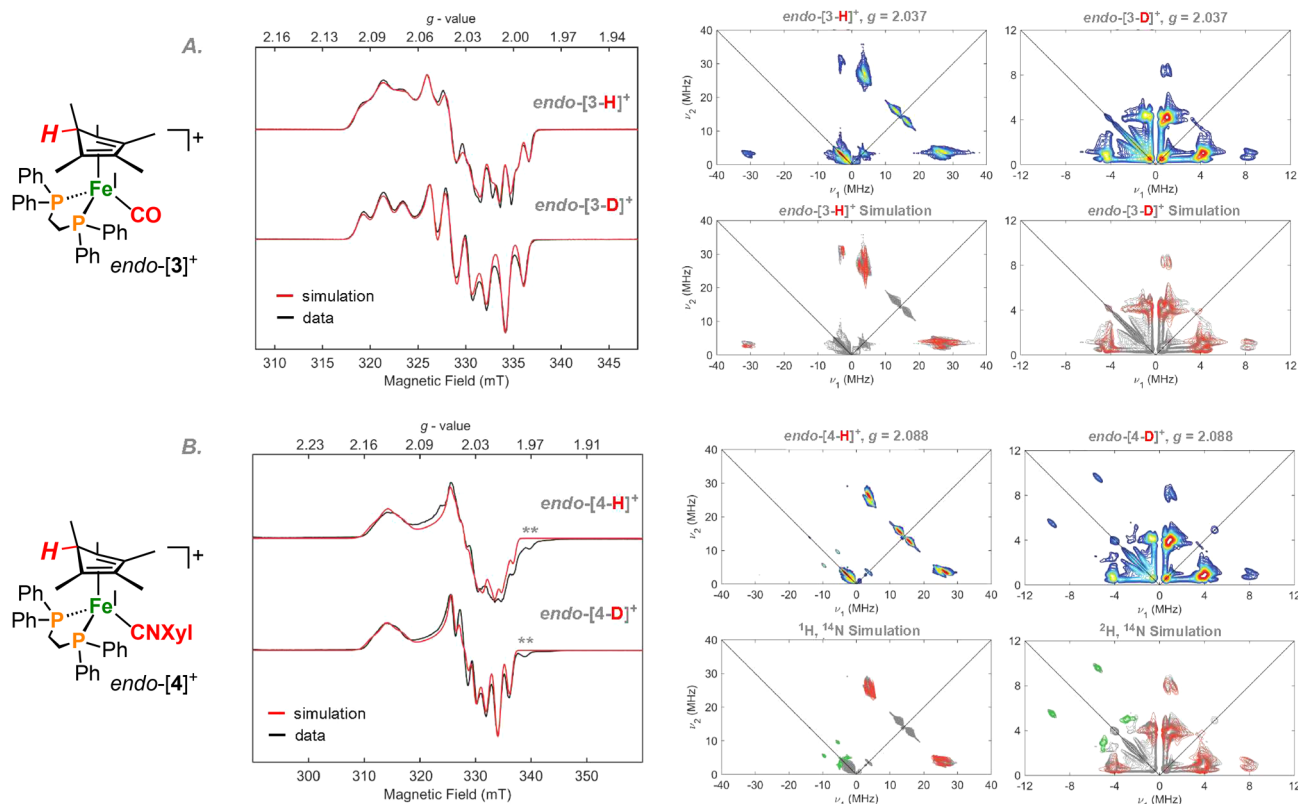


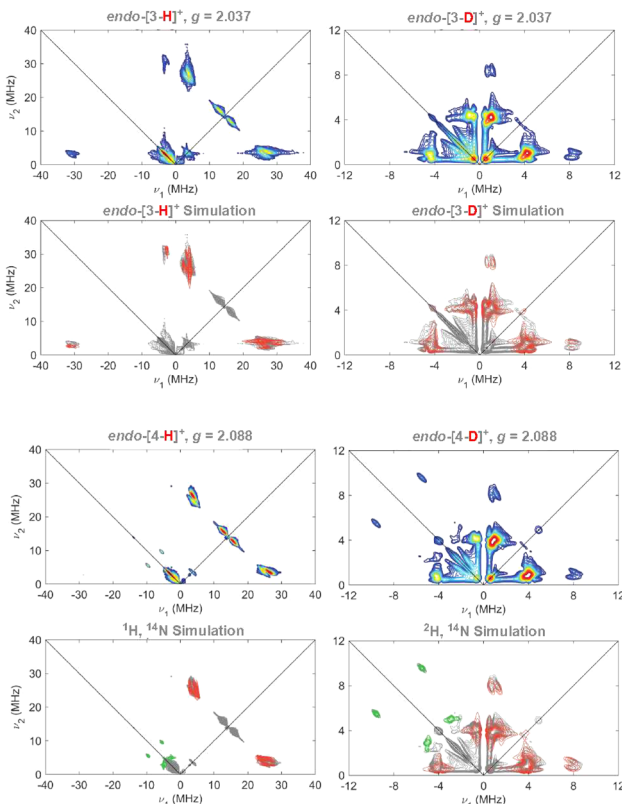
Figure 2. X-band CW-EPR spectra and corresponding X-band HYSCORE spectra of freeze-quenched samples in 2-MeTHF. (A) *endo*-[3-H]BAR^F₄ and *endo*-[3-D]BAR^F₄; (B) *endo*-[4-H]BAR^F₄ and *endo*-[4-D]BAR^F₄. HYSCORE simulations of features from ¹H, ²H (red), and ¹⁴N (green, CNXyl only) hyperfine couplings are overlaid over the data, which is plotted in gray. ** = traces of [1]⁺.

44, 15] MHz, and $A(^3P_2) = \pm[70, 64, 64]$ MHz for conformer B. The $a_{\text{iso}}(^1H)$ values for these isomers are much larger than that observed for the *endo* adduct, *endo*-[3]⁺ ($a_{\text{iso}}(^1H) = \pm 26.2$ MHz), while the magnitude of $T(^1H)$ tensors are similar to that observed for *endo*-[3]⁺ and are consistent with a ligand C–H, rather than M–H unit. This trend, $a_{\text{iso}}(^1H)$ (*exo*) > $a_{\text{iso}}(^1H)$ (*endo*) is also been observed for the protonated [Cp*(*endo/exo*- η^4 -Cp*H)Co]^{II} derivative (Figure 4) and correlates with greater predicted spin density on the *exo* (versus the *endo*) hydrogen atom for the staggered¹⁶ isomers (0.06 versus 0.02 e^-).

Annealing frozen solutions of the 17-electron η^4 -Cp*H complexes *endo*-[3]⁺, *exo*-[3]⁺, or *endo*-[4]⁺ (Scheme 1) provides *ca.* 0.5 equiv H₂ and their corresponding 18-electron $S = 0$ stable adducts, [Fe^{II}(η^5 -Cp*)(dppe)(CY)][BAR^F₄] ([5]BAR^F₄ (Y = O), [6]BAR^F₄ (Y = NXyl)). The Fe^{II}–CO adduct [5]⁺ has been described previously;¹⁷ full characterization data for [6]BAR^F₄ is in the Supporting Information. By contrast to *endo*-[3]⁺, which can be isolated and characterized at temperatures below –70 °C, H₂ evolution and formation of [5]⁺ from *exo*-[3]⁺ is observed at temperatures as low as –100 °C. As previously noted, the difference in stability between *endo*-[3]⁺ and *exo*-[3]⁺ is likely due to a dramatic difference in steric hindrance between the *endo*- and *exo*-H positions.

To gauge the relative energies of the species discussed herein, we turned to DFT calculations to estimate relevant BDFEs (Scheme 2). The starting hydride complex [1]⁺ was calculated to have a BDFE_{Fe–H} of 56 kcal mol^{–1}, providing the vacant $S = 1$ cation, [Fe(η^5 -Cp*)(dppe)]⁺ (III).

Associative binding of an L-type donor (prior to H[•] loss) was then considered. In this way, the CO (*endo*-[3]⁺) and



CNXyl (*endo*-[4]⁺) adducts, IV were calculated to be –3 and +3 kcal mol^{–1} in energy relative to [1]⁺. The process involves adduct formation and then reductive C–H elimination (or vice versa). H₂ formation from IV to give complexes VI ([5]⁺ and [6]⁺) is calculated to be highly favorable (CO and CNXyl: BDFE_{C–H} = 29 kcal mol^{–1} vs BDFE_{H–H} = 102.3 kcal mol^{–1} in CH₃CN)¹, correlating with a decrease in BDFE_{X–H} of almost 30 kcal mol^{–1} (cf. 56 kcal mol^{–1} for [1]⁺). The BDFE_{C–H} of *exo*-[3]⁺ is calculated to be weaker (25 kcal mol^{–1}), which in combination with the reduced steric crowding, manifests experimentally via facile H₂ evolution at temperatures for which *endo*-[3]⁺ is stable enough to isolate.

To experimentally benchmark the H[•] transfer propensity of [1]⁺, we aimed to determine an upper limit for its BDFE_{Fe–H}. Given the reduced Fe^{II}–H congener undergoes hydride transfer to 1-benzyl-3-acetamidopyridinium [BNAP]OTf ($\Delta G_{\text{H}} \approx 59$ kcal mol^{–1})¹⁸ and its known Fe^{II}/Fe^{III} oxidation potential ($E_{1/2} = -0.71$ V vs Fc/Fc⁺),¹⁹ the Fe^{III}–H bond of [1]⁺ is estimated to have an upper bound of BDFE_{Fe–H} < 50 kcal mol^{–1};²⁰ this can be compared with a DFT-predicted value of 56 kcal mol^{–1}. In spite of its weak BDFE_{Fe–H}, complex [1]⁺ is stable at room temperature in ethereal solvents (THF, Et₂O; <5% yield of H₂ and [Fe(η^5 -Cp*)(dppe)(N₂)]⁺ [7]⁺ at +80 °C, 1 week; Scheme 3); details pertaining to the characterization of [7]⁺ are presented in the Supporting Information. Although [7]⁺ is thermodynamically poised to release H₂, a substantial kinetic barrier presumably attenuates the rate of H₂ loss (BDFE_{H–H} = 102.3 kcal mol^{–1}).

Subsequently, we aimed to determine an upper limit for the BDFE_{C–H} of *endo*-[3]⁺ (Scheme 4). Reaction of an MeCN solution of *endo*-3 with CO₂ results in hydride transfer and

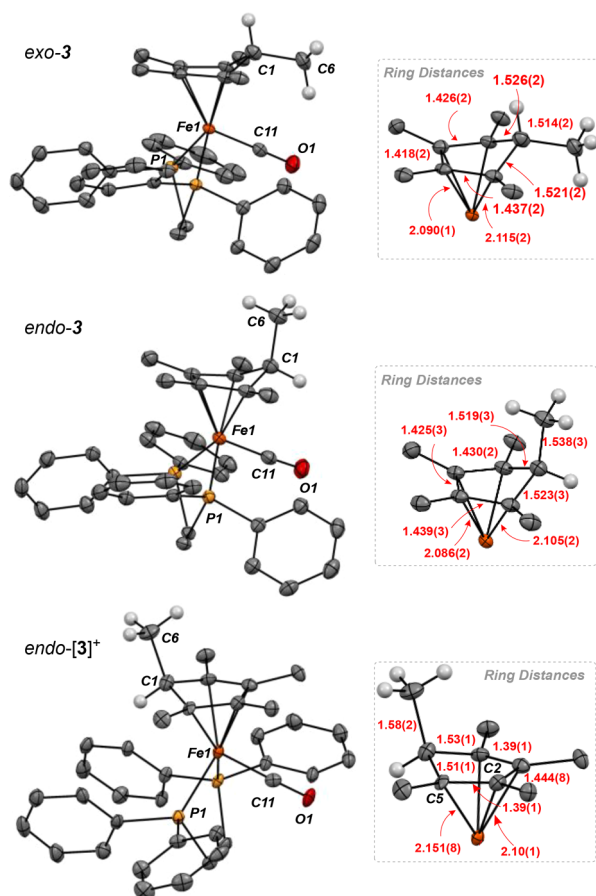


Figure 3. Solid-state structure of *exo-3*, *endo-3*, and *endo-[3]⁺* with ellipsoids shown at 50% probability. Counteranion omitted for *endo-[3]⁺*.

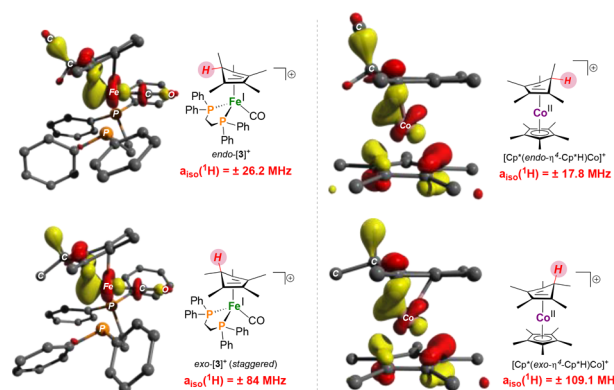


Figure 4. Frontier molecular orbitals (SOMOs) of *endo/exo-[3]⁺* (staggered conformers) and $[\text{Cp}^*(\text{endo/exo-}\eta^4\text{-Cp}^*\text{H})\text{Co}^{\text{II}}]^+_{7,8}$ optimized using TPSS; def2tvpz (Fe), def2svp (all other atoms). Inset shows $a_{\text{iso}}(^1\text{H})$ as obtained by ^1H HYSCORE and/or ENDOR.

formation of $[\text{Fe}(\eta^5\text{-Cp}^*)(\text{dppe})(\text{CO})]^+ [5]^+$. The hydricity of *endo-3* in MeCN must therefore be less than the hydricity of HCO_2^- ($\Delta G_{\text{H}^-} \approx 43 \text{ kcal mol}^{-1}$). In other words, *endo-3* is more hydric than HCO_2^- .²¹ Utilizing thermodynamic relationships that relate H^\bullet and H^- transfer in MeCN,²² the upper bound for the free energy of H^- transfer from *endo-3* and H^\bullet transfer from *endo-[3]⁺* can then be related. The $\text{endo-Cp}^*(\text{C-H})$ bond of *endo-[3]⁺* ($\text{Fe}^{0/1}$, $E_{1/2} = -0.81 \text{ V vs Fc/Fc}^+$) is thus conservatively estimated to have an upper bound

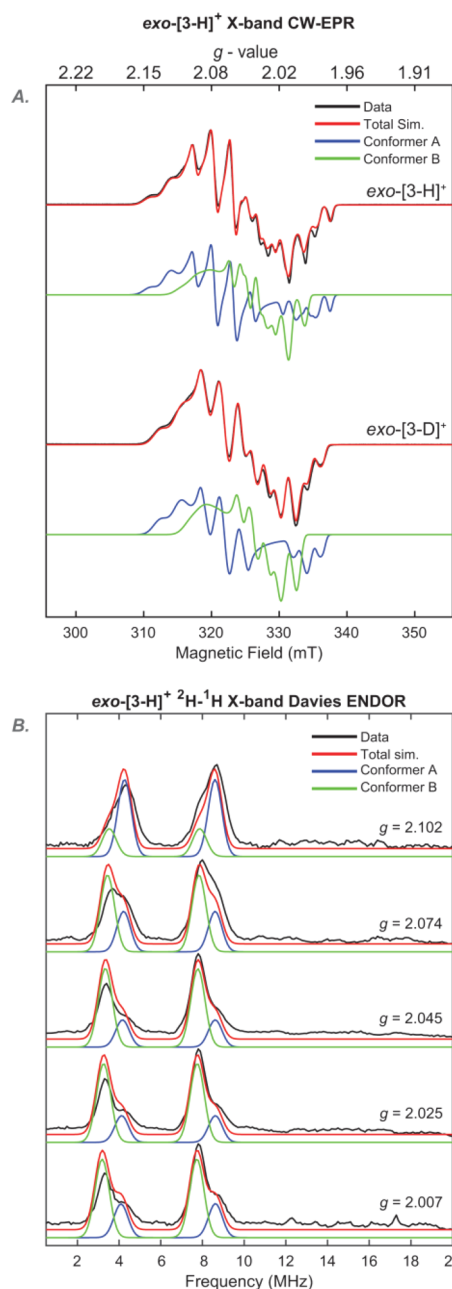
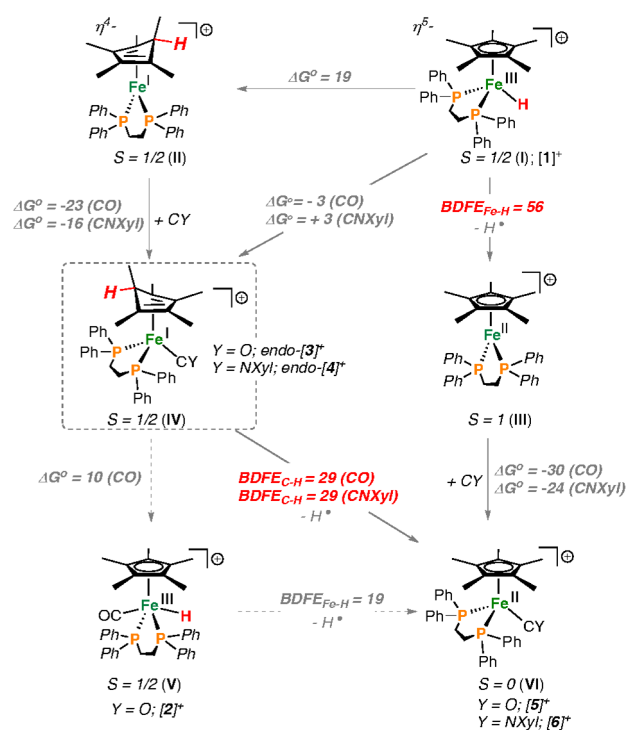


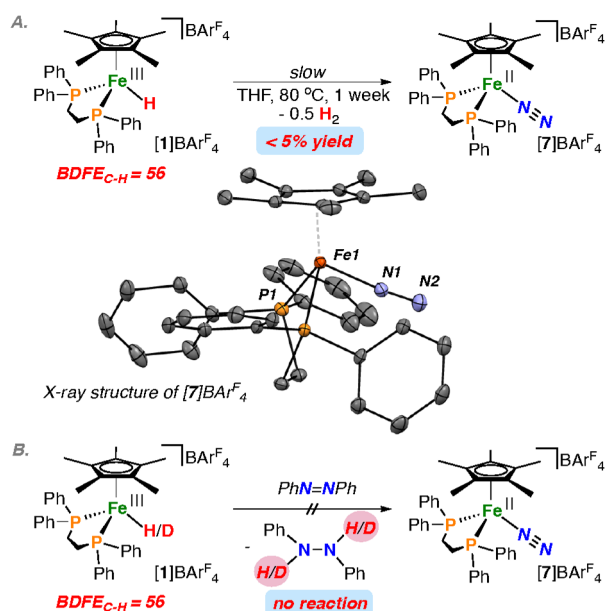
Figure 5. (A) X-Band CW-EPR spectra of freeze-quenched samples of *exo-[3-H/D]⁺* in 2-MeTHF at 77 K for with simulations of conformers A and B. (B) X-band $^2\text{H}-^1\text{H}$ Difference Davies ENDOR of *exo-[3-H]⁺* with data (black), total ^2H simulation (red), conformer A (blue), and conformer B (green).

BDFE ($\Delta G([3]^+)_{\text{H}\bullet}$) of $<36 \text{ kcal mol}^{-1}$ (DFT prediction: 29 kcal mol^{-1}), generating $[5]^+$ and H^\bullet as products. On the basis of thermodynamics alone, H_2 elimination from *endo-[3]⁺* should be facile. The experimentally predicted upper bound for the hydricity of *endo-[3]⁺* results in a pK_a of 23 in acetonitrile (see the Supporting Information for square scheme). In line with the predicted lower BDFE of *exo-[3]⁺*, its $\text{Fe}^{0/1}$ redox potential is more positive ($E_{1/2} = -0.70 \text{ V vs Fc/Fc}^+$) compared to *endo-[3]⁺*. This $\sim 110 \text{ mV}$ difference between the *endo* and *exo* isomers corresponds to a $\sim 2.5 \text{ kcal mol}^{-1}$ difference in BDFE, suggesting that an additional contributing factor to the difference in C-H BDFE's between these isomers is due to their different acidities.

Scheme 2. Free Energy Change (kcal mol⁻¹) for PCET Involving *endo*-[3]⁺/[4]⁺ [TPSS; def2tzvp (Fe), def2svp (All Other Atoms)]



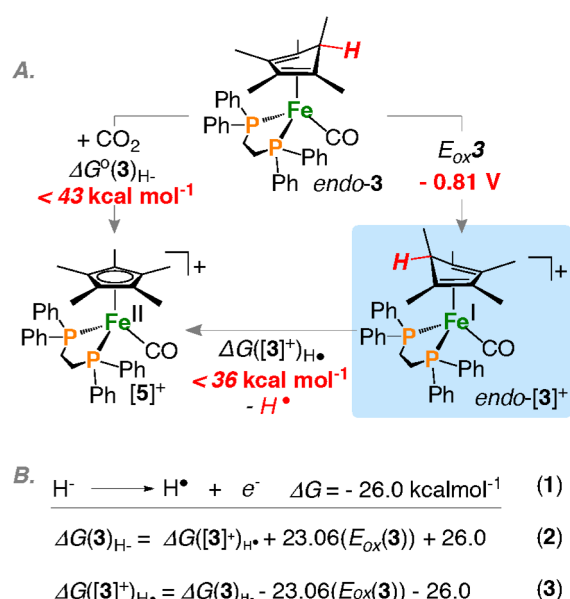
Scheme 3. (A) Synthesis of [7]⁺ by H₂ Evolution (<5%^a and (B) Non-Productive H[•] Transfer to Azobenzene Using [1]⁺^b



^aInset shows solid-state structure of [7]⁺ with ellipsoids shown at 50% probability. ^bBDFE values (kcal mol⁻¹) calculated by DFT using TPSS; def2tzvp (Fe), def2svp (all other atoms).

We next turned our focus to exploring whether a productive H[•] transfer to an exogenous substrate from either *endo*-[3]⁺ or *exo*-[3]⁺ could be accomplished, as opposed to undesired H₂ evolution. Azobenzene proved an interesting choice of substrate for this purpose as its conversion to diphenylhy-

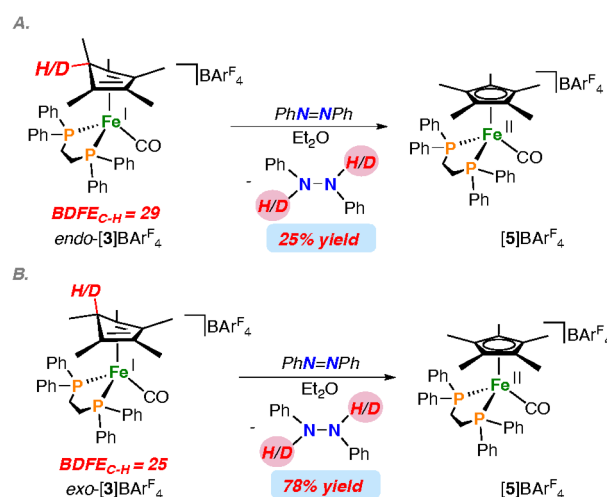
Scheme 4. (A) Experimental Determination of BDFE_{C-H} for *endo*-[3]⁺; (B) Relevant Thermodynamic Equations Relating H⁻ and H[•] Transfer for the *endo*-Variant Only



drazine and vice versa has been studied over the years with various PCET donors and acceptors,^{2,3} with some donors in a similar BDFE range.³

Complex [1]⁺ does not react with a 20-fold excess of azobenzene (PhN=NPh) over a period of days (for an average BDFE_{N-H} = 65 kcal mol⁻¹ over two transfers), but upon addition of CO, which generates *endo*-[3]⁺ in situ at -78 °C, a reaction is triggered to generate 1,2-diphenylhydrazine (25% yield, Scheme 5), H₂, and [5]⁺. Isotopic labeling studies using the deuterated analogue, *endo*-[3-D]⁺, result in the formation of the labeled isotopologue, PhDN-NDPh. In situ generation of *exo*-[3]⁺ through oxidation of *exo*-3 and reaction with PhN=NPh produces 1,2-diphenylhydrazine in 78% yield

Scheme 5. PCET Transfers to Azobenzene Using (A) *endo*-[3]⁺, Generating 25% PhNHNHPh, and (B) *exo*-[3]⁺, Giving 78% PhNHNHPh^a



^aBDFE values (kcal mol⁻¹) calculated by DFT using TPSS; def2tzvp (Fe), def2svp (all other atoms).

(Scheme 5). In line with *endo*-[3]⁺, only H₂ and [5]⁺ are observed as by products, and labeling with deuterium results in the formation of PhDN-NDPh. No other organic or iron containing products can be detected by NMR spectroscopy. A proton transfer followed by electron transfer or *vice versa* is unlikely as *endo* and *exo*-[3]⁺ are weak acids (vide supra), and the protonation step is calculated to be 27 kcal mol⁻¹ uphill. Furthermore, *endo* and *exo*-[3]⁺ are weak reductants ($E_{1/2} > -0.81$ V vs Fc/Fc⁺)²⁴ and not capable of reducing azobenzene to the radical anion ($E_{1/2} = -1.73$ V vs Fc/Fc⁺).²⁵ It is worth emphasizing that the increase in reaction rate upon addition of CO to [1]⁺ is orders of magnitude larger, as no H₂ formation or reduction of azobenzene is observed at room temperature in the absence of added CO, while instantaneous formation of [5]⁺, the terminal product of H[•] transfer, can be observed even at -78 °C. This remarkable difference in reactivity via addition of a simple L-type ligand highlights the potential for in situ generation of a powerful PCET reagent.

CONCLUSION

In closing, building on recent work describing protonated metallocene and related species with very weak and hence reactive C–H bonds, we have herein described the characterization of *endo*-[Fe^I(η⁴-Cp*H)(dppe)(L)]⁺ (L = CO, CNXyl) and *exo*-[Fe^I(η⁴-Cp*H)(dppe)(L)]⁺ (L = CO). Notably, one of these systems, *endo*-[Fe^I(η⁴-Cp*H)(dppe)(CO)]⁺, was previously studied but had been instead assigned as the 19-electron hydride species [Fe^{III}(η⁵-Cp*)(dppe)(CO)(H)]⁺. Use of pulse EPR techniques (^{1,2}H HYSCORE, ENDOR) as well as the solid-state crystal structure of *endo*-[Fe^I(η⁴-Cp*H)(dppe)(CO)]⁺, obtained at low temperature, cements this reassignment.

Our interest in these particular *endo*-[Fe^I(η⁴-Cp*H)(dppe)(L)]⁺ systems is that they can be generated in situ via L addition to a far more stable iron hydride precursor, [Fe^{III}(η⁵-Cp*)(dppe)H]⁺. This affords the opportunity to transfer H[•] to a substrate, demonstrated for L = CO using the reduction of azobenzene to diphenylhydrazine as a model, where the H[•] transfer reaction is triggered at low temperature via the addition of CO to a mixture of [Fe^{III}(η⁵-Cp*)(dppe)H]⁺ and PhN=NPh. The latter two partners do not otherwise react under the same conditions; CO triggers the isomerization that leads to the weak and hence reactive C–H bond. This approach demonstrates an attractive strategy for designing a powerful, in situ generated PCET reagent (BDFE_{C–H} ≈ 29 kcal mol⁻¹ for *endo*-[Fe^I(η⁴-Cp*H)(dppe)(CO)]⁺), with tunability of the BDFE via the choice of L donor.

ASSOCIATED CONTENT

Supporting Information

The Supporting Information is available free of charge at <https://pubs.acs.org/doi/10.1021/jacs.0c09363>.

Additional experimental details including figures, tables, and references as discussed in the text (PDF)

Crystallographic data for *exo/endo*-3, [3]BAR₄^F, [6]-BAR₄^F, and [7]BAR₄^F. CCDC 1943147–1943149 and 2021150–2021151 (CIF)

¹H, ¹³C{¹H}, and ³¹P{¹H} NMR spectra for complexes; Mössbauer, UV–vis, IR, and EPR spectroscopy; and computational models (MOL)

AUTHOR INFORMATION

Corresponding Author

Jonas C. Peters – Division of Chemistry and Chemical Engineering, California Institute of Technology, Pasadena, California 91125, United States; orcid.org/0000-0002-6610-4414; Email: jpeters@caltech.edu

Authors

Dirk J. Schild – Division of Chemistry and Chemical Engineering, California Institute of Technology, Pasadena, California 91125, United States

Marcus W. Drover – Division of Chemistry and Chemical Engineering, California Institute of Technology, Pasadena, California 91125, United States; orcid.org/0000-0002-2186-1040

Paul H. Oyala – Division of Chemistry and Chemical Engineering, California Institute of Technology, Pasadena, California 91125, United States; orcid.org/0000-0002-8761-4667

Complete contact information is available at: <https://pubs.acs.org/doi/10.1021/jacs.0c09363>

Author Contributions

[†]D.J.S. and M.W.D. contributed equally.

Notes

The authors declare no competing financial interest.

ACKNOWLEDGMENTS

The authors are grateful to the Department of Energy Basic Energy Sciences for support via Grant No. DOE-0235032. The Caltech EPR facility was previously supported by the National Science Foundation via Grant No. NSF MRI-153194 and is currently supported by the Dow Next Generation Educator Fund. The Beckman Institute is thanked for X-ray support. M.W.D. acknowledges NSERC (Banting PDF award), and M.W.D. and D.J.S. thank the Resnick Sustainability Institute at Caltech for fellowships.

REFERENCES

- (1) (a) Warren, J. J.; Tronic, T. A.; Mayer, J. M. Thermochemistry of Proton-Coupled Electron Transfer Reagents and its Implications. *Chem. Rev.* **2010**, *110*, 6961. (b) Weinberg, D. R.; Gagliardi, C. J.; Hull, J. F.; Murphy, C. F.; Kent, C. A.; Westlake, B. C.; Paul, A.; Ess, D. H.; McCafferty, D. G.; Meyer, T. J. Proton-Coupled Electron Transfer. *Chem. Rev.* **2012**, *112*, 4016. (c) Hammes-Schiffer, S. Theory of Proton-Coupled Electron Transfer in Energy Conversion Processes. *Acc. Chem. Res.* **2009**, *42*, 1881. (d) Gentry, E. C.; Knowles, R. R. Synthetic Applications of Proton-Coupled Electron Transfer. *Acc. Chem. Res.* **2016**, *49*, 1546. (e) Matos, J. L. M.; Green, S. A.; Shenvi, R. A. Markovnikov Functionalization by Hydrogen Atom Transfer. *Organic Reactions* **2019**, *100*, 383. (f) Tsui, E.; Metrano, A. J.; Tsuchiya, Y.; Knowles, R. R. Catalytic Hydroetherification of Unactivated Alkenes Enabled by Proton-Coupled Electron Transfer. *Angew. Chem., Int. Ed.* **2020**, *59*, 11845. (g) Roos, C. B.; Demareel, J.; Graff, D. E.; Knowles, R. R. Enantioselective Hydroamination of Alkenes with Sulfonamides Enabled by Proton-Coupled Electron Transfer. *J. Am. Chem. Soc.* **2020**, *142*, 5974. (h) Kolmar, S. S.; Mayer, J. M. SmI₂(H₂O)_n Reduction of Electron Rich Enamines by Proton-Coupled Electron Transfer. *J. Am. Chem. Soc.* **2017**, *139*, 10687. (2) Crossley, S. W. M.; Obradors, C.; Martinez, R. M.; Shenvi, R. A. Mn-, Fe-, and Co-Catalyzed Radical Hydrofunctionalizations of Olefins. *Chem. Rev.* **2016**, *116*, 8912.

- (3) Bezdek, M. J.; Guo, S.; Chirik, P. J. Coordination-induced weakening of ammonia, water, and hydrazine X–H bonds in a molybdenum complex. *Science* **2016**, *354*, 730.
- (4) Chalkley, M. J.; Garrido-Barros, P.; Peters, J. C. A molecular mediator for reductive concerted proton-electron transfers via electrocatalysis. *Science* **2020**, *369*, 850.
- (5) (a) Chciuk, T. V.; Anderson, W. R.; Flowers, R. A., II. High-Affinity Proton Donors Promote Proton-Coupled Electron Transfer by Samarium Diiodide. *Angew. Chem., Int. Ed.* **2016**, *55*, 6033. (b) Chciuk, T. V.; Anderson, W. R.; Flowers, R. A., II. Proton-Coupled Electron Transfer in the Reduction of Carbonyls by Samarium Diiodide-Water Complexes. *J. Am. Chem. Soc.* **2016**, *138*, 8738. (c) Chciuk, T. V.; Anderson, W. R., jr.; Flowers, R. A., II. Interplay between Substrate and Proton Donor Coordination in Reductions of Carbonyls by SmI₂-Water Through Proton-Coupled-Electron Transfer. *J. Am. Chem. Soc.* **2018**, *140*, 15342.
- (6) Ashida, Y.; Arashiba, K.; Nakajima, K.; Nishibayashi, Y. Molybdenum-catalyzed ammonia production with samarium diiodide and alcohols or water. *Nature* **2019**, *568*, 536.
- (7) (a) Chalkley, M.; Del Castillo, T.; Matson, B.; Roddy, J.; Peters, J. C. Catalytic N₂-to-NH₃ Conversion by Fe at Lower Driving Force: A Proposed Role for Metallocene-Mediated PCET. *ACS Cent. Sci.* **2017**, *3*, 217. (b) Chalkley, M. J.; Del Castillo, T. J.; Matson, B.; Peters, J. C. Fe-Mediated Nitrogen Fixation with a Metallocene Mediator: Exploring pK_a Effects and Demonstrating Electrocatalysis. *J. Am. Chem. Soc.* **2018**, *140*, 6122.
- (8) Chalkley, M. J.; Oyala, P. H.; Peters, J. C. Cp* Noninnocence Leads to a Remarkably Weak C-H bond via Metallocene protonation. *J. Am. Chem. Soc.* **2019**, *141*, 4721.
- (9) Drover, M. W.; Schild, D. J.; Oyala, P. H.; Peters, J. C. Snapshots of a Migrating H-Atom: Characterization of a Reactive Iron(III) Indenide Hydride and its Nearly Isoenergetic Ring-Protonated Iron(I) Isomer. *Angew. Chem., Int. Ed.* **2019**, *58*, 15504.
- (10) Hamon, P.; Toupet, L.; Hamon, J. R.; Lapinte, C. Novel diamagnetic and paramagnetic iron(II), iron(III), and iron(IV) classical and nonclassical hydrides. X-ray crystal structure of [Fe(C₅Me₅)(dppe)D]PF₆. *Organometallics* **1992**, *11*, 1429.
- (11) Hamon, P.; Hamon, J. R.; Lapinte, C. Isolation and characterization of a cationic 19-electron iron(III) hydride complex; electron transfer induced hydride migration by carbon monoxide at an iron(III) center. *J. Chem. Soc., Chem. Commun.* **1992**, 1602.
- (12) For example: (a) Chiang, K. P.; Scarborough, C. C.; Horitani, M.; Lees, N. S.; Ding, K.; Dugan, T. R.; Brennessel, W. W.; Bill, E.; Hoffman, B. M.; Holland, P. L. Characterization of the Fe-H Bond in a Three-Coordinate Terminal Hydride Complex of Iron(I). *Angew. Chem., Int. Ed.* **2012**, *51*, 3658. (b) Gu, N. X.; Oyala, P. H.; Peters, J. C. An S = 1/2 Iron Complex Featuring N₂, Thiolate, and Hydride Ligands: Reductive Elimination of H₂ and Relevant Thermochemical Fe-H Parameters. *J. Am. Chem. Soc.* **2018**, *140*, 6374.
- (13) Lucken, E. A. C. *Nuclear Quadrupole Coupling Constants*; Academic Press: London, 1969; pp 227–131.
- (14) For the IR spectrum of free Cp*H, see: Threlkel, R. S.; Bercaw, J. E.; Seidler, P. F.; Stryker, J. M.; Bergman, R. G. 1,2,3,4,5-pentamethylcyclopentadiene. *Org. Synth.* **1987**, *65*, 42.
- (15) Green, M. L. H.; Pratt, L.; Wilkinson, G. 760. A new type of transition metal–cyclopentadiene compound. *J. Chem. Soc.* **1959**, *0*, 3753–3767.
- (16) Here, staggered refers to the puckered CH(CH₃) group as being on the opposite side of the [Fe]-coordinated CO ligand.
- (17) (a) Paul, F.; Toupet, L.; Roinsel, T.; Hamon, P.; Lapinte, C. Solid-state characterisation of the [(η²-dppe)(η⁵-C₅Me₅)FeCO]⁺ cation: an unexpected ‘oxidation’ product of the [(η²-dppe)(η⁵-C₅Me₅)FeC = C(C₆H₄)NMe₂]⁺ radical cation. *C. R. Chim.* **2005**, *8*, 1174. (b) Catheline, D.; Astruc, D. Synthesis and characterization of C₅(CH₃)₅Fe(CO)₃⁺PF₆[−] and C₅(CH₃)₅Fe(CO)₂[−]K⁺. *J. Organomet. Chem.* **1982**, *226*, No. c52.
- (18) In the reaction between [Fe(η⁵-Cp*)(dppe)(H)] and [BNAP]⁺, the solvent adduct, [Fe(η⁵-Cp*)(dppe)(NCMe)]⁺, and BNAPH are produced, in this case, acetonitrile binding will cause the experimentally determined BDFE (50 kcal mol^{−1}) to be lower by as much as the binding strength of MeCN to the vacant Fe(II) complex, [Fe(η⁵-Cp*)(dppe)]⁺. By DFT, we estimate this value to be 12 kcal mol^{−1}, bringing the BDFE to 62 kcal mol^{−1}. See: Zhang, F.; Jia, J.; Dong, S.; Wang, W.; Tung, C.-H. Hydride Transfer from Iron(II) Hydride Compounds to NAD(P)⁺ Analogues. *Organometallics* **2016**, *35*, 1151.
- (19) Tilset, M.; Fjeldahl, I.; Hamon, J.-R.; Hamon, P.; Toupet, L.; Saillard, J.-Y.; Costuas, K.; Haynes, A. Theoretical, Thermodynamic, Spectroscopic, and Structural Studies of the Consequences of One-Electron Oxidation on the Fe-X Bonds in 17- and 18-Electron Cp*Fe(dppe)X Complexes (X = F, Cl, Br, I, H, CH₃). *J. Am. Chem. Soc.* **2001**, *123*, 9984.
- (20) This value does not take into account the free energy associated with acetonitrile binding.
- (21) (a) Ilic, S.; Pandey Kadel, U.; Basdogan, Y.; Keith, J. A.; Glusac, K. D. Thermodynamic Hydricities of Biomimetic Organic Hydride Donors. *J. Am. Chem. Soc.* **2018**, *140*, 4569. (b) Ellis, W. W.; Raebiger, J. W.; Curtis, C. J.; Bruno, J. W.; DuBois, D. L. Hydricities of BzNADH, C₅H₅Mo(PMe₃)(CO)₂H, and C₅H₅Mo(PMe₃)(CO)₂H in Acetonitrile. *J. Am. Chem. Soc.* **2004**, *126*, 2738.
- (22) (a) Wiedner, E. S.; Chambers, M. B.; Pitman, C. L.; Bullock, R. M.; Miller, A. J. M.; Appel, A. M. Thermodynamic hydricity of Transition Metal Hydrides. *Chem. Rev.* **2016**, *116*, 8655. (b) Pearson, R. G. The Transition-Metal-Hydrogen Bond. *Chem. Rev.* **1985**, *85*, 41.
- (23) (a) Savéant, J.-M.; Tard, C. Proton-Coupled Electron Transfer in Azobenzene/Hydrazobenzene Couples with pendant Acid-Base Functions. Hydrogen-Bonding and Structural Effects. *J. Am. Chem. Soc.* **2014**, *136*, 8907. (b) Cattaneo, M.; Ryken, S. A.; Mayer, J. M. Outer-Sphere 2e[−]/2H⁺ Transfer Reactions of Ruthenium(II)-Amine and Ruthenium(IV)-Amido Complexes. *Angew. Chem., Int. Ed.* **2017**, *56*, 3675.
- (24) The Fe^{II/I} redox potential of *endo* and *exo*-[3]⁺ could not be determined experimentally but the Fe^{I/0} couples give conservative lower limits of, respectively, −0.81 and −0.70 V vs Fc/Fc⁺.
- (25) Goulet-Hanssens, A.; Utecht, M.; Mutruc, D.; Titov, E.; Schwarz, J.; Grubert, L.; Bleger, D.; Saalfrank, P.; Hecht, S. Electrocatalytic Z – > E Isomerization of Azobenzenes. *J. Am. Chem. Soc.* **2017**, *139*, 335–341.